IOP PUBLISHING PHYSICS IN MEDICINE AND BIOLOGY

Phys. Med. Biol. **54** (2009) 1089–1109 doi:10.1088/0031-9155/54/5/001

pH-induced contrast in viscoelasticity imaging of biopolymers

R D Yapp and M F Insana

Department of Bioengineering, Beckman Institute for Advanced Science and Technology, University of Illinois, Urbana-Champaign, IL 61801, USA

E-mail: ryapp2@illinois.edu

Received 13 June 2008, in final form 19 December 2008
Published 27 January 2009
Online at stacks.iop.org/PMB/54/1089

Abstract

Understanding contrast mechanisms and identifying discriminating features is at the heart of diagnostic imaging development. This paper focuses on how pH influences the viscoelastic properties of biopolymers to better understand the effects of extracellular pH on breast tumour elasticity imaging. Extracellular pH is known to decrease as much as 1 pH unit in breast tumours, thus creating a dangerous environment that increases cellular mutatation rates and therapeutic resistance. We used a gelatin hydrogel phantom to isolate the effects of pH on a polymer network with similarities to the extracellular matrix in breast stroma. Using compressive unconfined creep and stress relaxation measurements, we systematically measured the viscoelastic features sensitive to pH by way of time-domain models and complex modulus analysis. These results are used to determine the sensitivity of quasi-static ultrasonic elasticity imaging to pH. We found a strong elastic response of the polymer network to pH, such that the matrix stiffness decreases as pH was reduced; however, the viscous response of the medium to pH was negligible. While physiological features of breast stroma such as proteoglycans and vascular networks are not included in our hydrogel model, observations in this study provide insight into viscoelastic features specific to pH changes in the collagenous stromal network. These observations suggest that the large contrast common in breast tumours with desmoplasia may be reduced under acidic conditions, and that viscoelastic features are unlikely to improve discriminability.

1. Introduction

Elasticity imaging continues to mature as a tool for breast cancer diagnosis because of its unique ability to describe mechanical properties of soft tissues. The excitement about diagnostic elasticity imaging stems from the large increase in stiffness (or equivalently a reduction in elastic strain) commonly associated with tumours. Specifically, elasticity imaging is able to

image the characteristic signature of desmoplasia that is often specific to malignancies (Garra *et al* 1997). Nevertheless, many early-stage lesions, some as large as 2 cm, do not change stiffness, which suggests a need to increase the mechanical feature space for diagnosis (Pellot-Barakat *et al* 2006, Qiu *et al* 2008). To realize the diagnostic potential of elasticity imaging, researchers must improve knowledge of the mechanisms by which breast diseases generate elasticity contrast.

Several groups are studying contrast mechanisms through different approaches to elasticity imaging. Each shares the aim of exploring viscoelastic (VE) properties of soft biological tissues for diagnosis. Quasi-static methods used by us and others (Ophir *et al* 1991, Doyley *et al* 2006, Khaled *et al* 2006) require that a constant stress is maintained on the tissue, while the materials strain response is monitored using ultrasound. In quasi-static elasticity imaging methods used in our laboratory (Sridhar and Insana 2007), a force on the order of 4 N is suddenly applied to tissues in about 1 s and held constant for 10–200 s while frames of radio frequency (RF) echo signals are recorded. The RF signals are analysed to track tissue movements and thus generate a time series of strain images. To estimate VE parameters, we fit rheological model functions obtained via constitutive equations to the time-varying strain data. The slow timing of the applied ramp-and-hold force means that stress stimuli are applied at very low frequencies (quasi-static), typically in a bandwidth below 1 Hz. Dynamic methods (Sharma *et al* 2004, Sinkus *et al* 2005, 2007, Tanter *et al* 2008), in contrast, apply much lower forces at much higher force–stimulation frequencies (>50 Hz), which is significant because hydrogels, including breast stroma and other connective tissues, exhibit frequency-dependent material properties (Ferry 1980). In this paper, we study the effects of pH on gelatin hydrogel dynamics at force frequencies between 10^{-3} and 10^{-1} rad s^{-1}. Our goal is to explore the sensitivity of quasi-static elasticity methods for imaging pH-sensitive VE properties in tissue-like media.

What occurs in breast tumours that could change VE properties? The answer originates with the molecular biology of cancer. Malignant mammary epithelial cells initiate a cascade of signaling pathways that interact with the extracellular matrix of breast stroma to stimulate tumour cell proliferation, differentiation, adhesion and concomitant support systems such as neoangiogenesis (Fata *et al* 2004). Breast stroma, the supporting matrix of mammary tissue that determines mechanical properties, is known to play an active role in processes leading to malignant progression (Elenbaas and Weinberg 2001). Depending on microenvironmental factors in the stroma, cell growth can be rapid and chaotic, thus producing heterogeneous, hypoxic neoplasms with acidic regions where growth has outpaced the nutrient supply and waste removal provided by regional blood flow. Irregular perfusion and increased lactic acid secretion by tumour cells produces pH gradients across cell membranes as large as 0.6 pH units (Gerweck *et al* 2006), and extracellular pH (pH_e) gradients up to 1 pH unit across a 1 cm distance (Gillies *et al* 2004). Acidic conditions are dangerous microenvironmental factors because they increase the rate of malignant cell transformation, *in vivo* metastasis, and the resistance to conventional therapeutics.

Variations in pH from the isoelectric pH (IEP) value[1] are also known to alter the matrix structure of many hydropolymers (Veis 1964), including connective tissues, and thus the VE properties (Usha and Ramasami 2000, Roeder *et al* 2002, Seehra and Silver 2006). Isolated extracellular matrix proteins have a net negative surface charge. They self-assemble *in situ* with conformations that seek stability near the IEP. We are investigating the role of pH on the VE properties of hydrogels so as to begin to understand its role in generating breast tumour elasticity contrast. The extracellular matrix of stroma undergoes a constant reorganization

[1] The IEP is the pH at which a polypeptide has zero net charge (Brown 2002).

and growth during cancer progression. Therefore, temporal variations in tumour pH_e are expected to generate a spatiotemporal modulation of structural extracellular matrix change. For hydrogels to be useful at modelling this situation, we need to modify the pH away from its IEP during polymerization.

Gelatin hydrogels were previously investigated as simple physical models of breast stroma in order to validate our elastic imaging techniques (Sridhar *et al* 2007a). Although there are major differences between the structures of gelatin and extracellular matrix polymers, comparisons of their VE properties show that gelatin hydrogels can be a reasonable model for breast tissues (Sridhar *et al* 2007b, Sridhar and Insana 2007). The fibril form of natural type I collagen in the stromal extracellular matrix is a highly ordered elastic structure, stabilized by hydrogen and electrostatic bonds within and among the proteins. In addition to the net negative surface charge, hydrophilic proteoglycan molecules aid in structuring fluid in the collagenous matrix (Stoeckelhuber *et al* 2002). In the denatured form of collagen, gelatin forms a less-ordered elastic aggregate network containing polar side chains that aid in structuring fluids to form a hydrogel.

The goal of this study is to determine the degree to which quasi-static elasticity imaging is sensitive to pH changes in hydrogels. In this experimental study, homogeneous gelatin gel samples are constructed at pH levels about the IEP and tested using classic mechanical techniques. The results from these studies are used to predict and understand sources of pH-induced contrast in gelatin gel phantoms imaged with ultrasonic elasticity imaging. Gel data are used to begin evaluating the role of pH changes in diseased breast stroma.

2. Governing equations and model descriptions

We performed two types of transient mechanical experiments on gelatin gels: creep and stress relaxation. Our primary focus was on creep because we can image the strain response. The stress relaxation experiment, which mechanically stimulates the gel with a strain rather than a stress, was used because it provides an alternative perspective of the material properties. In this study, creep tests took the form of unconfined uniaxial compression, where the stress is applied to the top surface of the sample in about 1 s and held for at least 1800 s. The ramp is approximated as a step function. These creep tests were performed on both the homogeneous gel samples and the elasticity imaging phantoms. The stress relaxation test was only performed on the homogeneous gel samples, and is also an unconfined uniaxial compression test, where the applied strain is assumed to be a step function as the strain is applied to the top surface of the sample in about 1 s and held for 3600 s. Detailed descriptions of the relevant constitutive equations for these experiments are described elsewhere (Sridhar *et al* 2007a). The constitutive equations were applied in the development of rheological models to parameterize creep data for imaging. The following descriptions are specific to results in this paper.

The constitutive equation for uniaxial compressive creep is given by

$$\varepsilon(t) = \int_0^t \frac{\partial \sigma(t')}{\partial t'} D(t - t')\, \mathrm{d}t', \tag{1}$$

where $\varepsilon(t)$ is the strain response along the axis of $\sigma(t)$, the uniaxial applied stress, and $D(t)$ is the compressive compliance. The frequency response $\tilde{\varepsilon}(\omega)$ of equation (1) is found from the Fourier transform,

$$\tilde{\varepsilon}(\omega) = \mathrm{i}\omega\tilde{\sigma}(\omega)\tilde{D}(\omega), \tag{2}$$

where $\tilde{\varepsilon}(\omega)$, $\tilde{\sigma}(\omega)$ and $\tilde{D}(\omega)$ are the Fourier transforms of $\varepsilon(t)$, $\sigma(t)$ and $D(t)$, respectively, and $\mathrm{i} = \sqrt{-1}$. The frequency-dependent material properties are described by the complex modulus $E^*(\omega)$, which is related to the transient experiments by equation (3), where $E'(\omega)$

and $E''(\omega)$ are the real and imaginary parts of $E^*(\omega)$, respectively (Tschoegl 1989, Fried 2003):

$$\mathrm{i}\omega\tilde{D}(\omega) = \frac{1}{E^*(\omega)} = \frac{1}{E'(\omega) + \mathrm{i}E''(\omega)}. \tag{3}$$

It is advantageous to analyse data in the frequency domain because it provides separable information about mechanical energy stored (real part) and lost (imaginary part) (Ferry 1980), which emphasizes the elastic and viscous components.

Since for creep experiments used in this study $\sigma(t) \cong \sigma_a u(t)$,[2] the compressive compliance $D(t)$ is simply $\varepsilon(t)/\sigma_a$. Also, $1/E^*(\omega)$ is estimated from the strain data by taking the Fourier transform of the derivative of $D(t)$.

Based upon previous experience with creep tests on gelatin gels, the time-domain strain response is well modelled by a generalized Voigt model. This complex polymer network likely has a contribution from a continuum of responses as described by equation (4). A discrete version of the model as shown in equation (5) is a good approximation that can be used to parameterize the material response by focusing only on the K largest eigenvalues (Sridhar *et al* 2007b). ε_0 is the strain amplitude of the initial elastic response, and the parameters ε_k and T_k represent the amplitudes and time constants of the VE components, respectively, for each discrete Voigt element. Previously (Sridhar *et al* 2007a, Yapp *et al* 2007) it was shown that a bi-exponential model with a linear component representing a purely viscous response ($\beta = \sigma_a/\eta_0$, where η_0 is the viscosity coefficient) was a good approximation to experimental data as seen in equation (6). However, new evidence suggests this linear component is a viscoelastic element with $T_3 \gg T_1, T_2$. Thus, in this study we modelled the creep response with a tri-exponential Voigt model with $\beta = \varepsilon_3/T_3$ representing the $k = 3$ viscoelastic component approximated from its first-order Taylor series expansion. This tri-exponential model was obtained from experimental data by first estimating and subtracting the linear component βt from the creep data, followed by fitting the time-domain strain data to a discrete bi-exponential Voigt model as described elsewhere (Sridhar *et al* 2007a, 2007b):

$$\varepsilon(t) = \varepsilon_0 + \int_0^t \mathrm{d}\tau \dot{\varepsilon}(\tau)\left(1 - \exp\left(-\frac{\tau}{T}\right)\right) \tag{4}$$

$$\simeq \varepsilon_0 + \sum_{k=1}^{K} \varepsilon_k \left(1 - \exp\left(-\frac{t}{T_k}\right)\right) \tag{5}$$

$$\simeq \varepsilon_0 + \sum_{k=1}^{2} \varepsilon_k \left(1 - \exp\left(-\frac{t}{T_k}\right)\right) + \beta t. \tag{6}$$

A similar analysis is applied to the stress relaxation test, which is assumed to have a step strain input $\varepsilon(t) = \varepsilon_a u(t)$. The constitutive equation governing the stress relaxation test is given in equation (7),

$$\sigma(t) = \int_0^t \frac{\partial \varepsilon(t')}{\partial t'} E(t - t')\,\mathrm{d}t', \tag{7}$$

where $E(t)$ is the compressive modulus. The complex modulus, $E^*(\omega)$, is estimated from the stress data by taking the Fourier transform of the derivative of $E(t) = \sigma(t)/\varepsilon_a$ as (Tschoegl 1989, Sridhar *et al* 2007a)

$$\mathfrak{F}\left\{\frac{\mathrm{d}}{\mathrm{d}t}E(t)\right\} = \mathrm{i}\omega\tilde{E}(\omega) = E^*(\omega) = E'(\omega) + \mathrm{i}E''(\omega), \tag{8}$$

where $\tilde{E}(\omega)$ is the Fourier transform of $E(t)$.

[2] $u(t)$ is the unit step function.

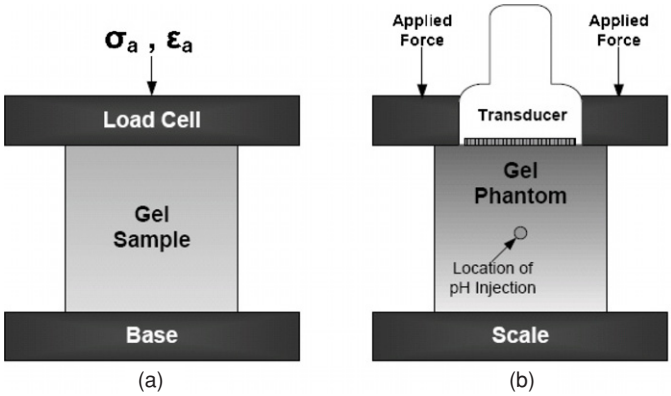

Figure 1. This figure displays schematics of the three experimental methods. Part (a) illustrates unconfined uniaxial compression (when the stimulus is stress this is a creep experiment, and when the stimulus is strain this is a stress relaxation experiment). Part (b) illustrates the elasticity imaging experiment.

The Fourier transforms of compliance and modulus from stress relaxation and creep experiments are related by $\tilde{D}(\omega)\tilde{E}(\omega) = 1/(\mathrm{i}\omega)^2$. The elastic modulus $E_0 = E(t = 0) = \sigma(t = 0)/\varepsilon_\mathrm{a}$ is found from stress relaxation data, and is related to the elastic compliance $D_0 = D(t = 0) = \varepsilon_0/\sigma_\mathrm{a} = 1/E_0$. $E^*(\omega)$ may be estimated from either experiment. The goal of this study is to estimate pH dependence on estimates of ε_k, T_k, E_0 and β for gelatin hydrogels.

Creep tests performed on homogeneous gel samples share the same experimental geometry as elasticity imaging studies. To avoid confusion, the results of creep experiments performed on homogeneous gel samples will be referred to as 'creep' measurements and those of elasticity imaging experiments will be referred to as 'elasticity imaging' measurements from this point forward. Contrast parameters found from the creep measurements are used as an aid for verifying and predicting imaging parameters in the elasticity imaging measurements. Information gained from stress relaxation data as well as $E^*(\omega)$ provides additional insight into the source of VE contrast with pH and is used as a tool for physical interpretation of imaging parameters.

3. Methods

3.1. Hydrogel samples

The three different experiments performed on gelatin gels are illustrated in figure 1. For creep and stress relaxation measurements, samples of the same shape were used (section 3.2); however, the elasticity imaging experiment used gel phantoms of a different shape and construction (section 3.3). To avoid confusion the gel samples for creep and stress relaxation measurements are referred to as 'gel samples', and gel samples for elasticity imaging are referred to as 'gel phantoms'. We found that mechanical properties of these gels are extremely sensitive to slight variations in thermal history during production, storage and experimentation. Effort was made to create gel samples in which the conditions were similar in order to better relate the results across experiments; the commonalities are described here.

All gelatin gel samples were constructed with 250 bloom strength, type B gelatin provided by Rousselot (Dubuque, IA). Type B gelatin is obtained from animal hides by an alkali hydrolysis reaction. The IEP of the particular gelatin used in this study is known to be in the range 4.8–5.2. Gel samples are comprised of 8% w/w gelatin, 91.9% w/w deionized water and 0.1% w/w formaldehyde. The formaldehyde is a 37% w/w solution purchased from Thermo Fisher Scientific (Waltham, MA). Under these conditions the pH of the hydrogel is 5.6. This pH is close to the IEP reported by the manufacturer. According to Hitchcock (1931), the pH of the gel will approach the gelatin IEP as the gelatin concentration in water increases. In this study, pH 5.6 is referred to as the IEP. The pH of the gels was lowered by adding a volume 1N HCl and raised using 1N NaOH as described below. A pH meter, model UP-5, equipped with a glass-body liquid filled micro combination electrode from Denver Instruments (Denver, CO) was used to measure the pH of the gels.

The combination of gelatin and water was heated in a water bath at 60 °C for 1 h and stirred every 10 min. Once the gelatin solution was removed from the heat, it was allowed to cool at room temperature (21–22 °C) to 50 °C before adding formaldehyde. Further sample preparation varied between the two types of gel samples as discussed below.

3.2. Gel samples for creep and stress relaxation measurements

The purpose of creating homogeneous gel samples at pH levels 4.6, 5.6 and 6.6 was to systematically study the mechanical properties of gelatin gels ±1 pH unit about the IEP. Creep measurements on these gels were used to determine pH-sensitive contrast parameters. Stress relaxation measurements provided an alternative method for analysing VE properties as a function of pH. Both measurements allowed estimation of $E^*(\omega)$ and associated VE parameters as a function of pH. At each pH level (pH 4.6, 5.6 and 6.6) four gelatin gel samples were created from a single batch: two samples were used for creep and two for stress relaxation. The room temperature from the time of sample construction until measurement did not vary more than 1 °C.

Gel samples constructed for the unconfined creep and stress relaxation tests were homogeneous cylinders of height and diameter 44.5 mm. After preparing the gel solution as described in section 3.1, HCl or NaOH was added as necessary to the gelatin solution immediately following the addition of formaldehyde. The solution was then further cooled to 40 °C before being poured into rigid plastic molds. Mold release (Pol-Ease 2300 by Polytek, Easton, PA) coats the inside of the mold to prevent adhesion of the gel with the plastic. The total polymerization time (t_p) is considered to be the time from which the gel is allowed to start cooling until the time the sample is tested. For these gels, $t_p = 48$ h at room temperature. The quantities of HCl and NaOH necessary to shift the gelatin solution pH were empirically determined by slowly adding the acid or base just after the addition of formaldehyde, while simultaneously monitoring the pH with the pH meter. These quantities are displayed in table 1. Based upon these findings, an asymmetric relationship is observed about the IEP in regard to the number of H^+ and OH^- ions needed to shift the pH. This observation is in agreement with previous studies of type B gelatin (Veis 1964).

3.3. Gel phantoms for elasticity imaging measurements

The purpose of this elasticity imaging study was to detect VE contrast due to spatial variations in gel pH in an otherwise homogeneous phantom. This was accomplished by creating a region at the centre of a gel cube that was allowed to polymerize in the presence of an acid or a base.

Table 1. The fraction by total sample weight of acid (1N HCl) or base (1N NaOH) that was added to gel solutions to achieve stated pH values. The specific gravity of the 1N HCl and 1N NaOH solutions is approximately 1.

pH	4.1	4.6	5.1	5.6	6.1	6.6	7.1
HCl (w/w)%	3.0	1.56	0.69	0	0	0	0
NaOH (w/w)%	0	0	0	0	0.31	0.56	0.75

Introduction of a localized pH change in the gel solution before polymerization to the gel state is intended to simulate changes in breast tissue stroma near acidic tumours.

Imaging phantoms were constructed using the gelatin solution as described in section 3.1. After the formaldehyde was added, the gelatin solution continued to cool at room temperature to 45 °C after which 3.35% w/w graphite was mixed thoroughly with a spoon. When the gel temperature reached 40 °C, the still molten solution was placed into a vacuum chamber for < 5 min to remove gasses introduced by the graphite suspension process. The solution was then poured into a mold and cooled at room temperature. The inside surfaces of a 50 mm cubic phantom mold case are coated with mold release, and one piece of PE-50 tubing (OD: 0.965 mm, ID: 0.58 mm) was inserted through the centre of opposing sides of the acrylic mold. The phantom case apparatus was attached to a rotation table and rotated at 1 rpm for approximately 2 h to prevent graphite settling as the gelatin solution polymerized.

Graphite was added to these phantoms to provide ultrasonic tissue-like scattering and absorption. In comparison with the creep and stress relaxation samples, we assume the effect of graphite on the gel mechanical properties is small. According to Hall *et al* (1997) graphite produces a small effect on gel stiffness giving an elastic modulus difference on the order of 1 kPa between a phantom with and without graphite at 5.5% w/w concentration.

After approximately 2 h of rotation, the gelatin solution was a very weakly polymerized gel. Fluids could freely diffuse in the highly viscous medium. At that time, the central region of the gel was introduced to an acid or base by slowly infusing the HCl or NaOH into the PE-50 tubing, while the tube was slowly withdrawn from the case at a relatively constant rate. The goal was to leave a uniform linear path of the acid or base that could quickly diffuse without also leaving a structural defect in the gel once it had fully congealed. After injection, the phantom quiescently congealed at room temperature for 48 h before measurement. Three phantoms were constructed: an acidic injection of 1N HCl, a control injection of deionized water mixed with HCl to have a pH of 5.6 and a basic injection of 1N NaOH.

3.4. Creep and stress relaxation measurements

Creep and stress relaxation measurements were performed on the gel samples described in section 3.2 using a TA.XT Plus Texture Analyzer System and a 1 kg load cell (Texture Technologies Corp., Scarsdale, NY). Displacement and force data were acquired at 10 samples s^{-1}. The top and bottom of the gel samples were coated with a thin layer of oil to provide free-slip conditions and minimize desiccation. The gels were compressed using a 3 inch diameter flat aluminum plate. An acrylic environmental box enclosed the analyser system to stabilize temperature and minimize air flow around the samples.

To determine the linear stress–strain range of the gel samples, a 30 g pre-load ($\sim$2% strain) followed by a cyclic triangular-wave pattern of loading and unloading an additional 10% strain at a period of 25 s was applied to the samples. These tests were performed using the analyser system. A pre-load was applied to minimize tensile forces between the compression plate

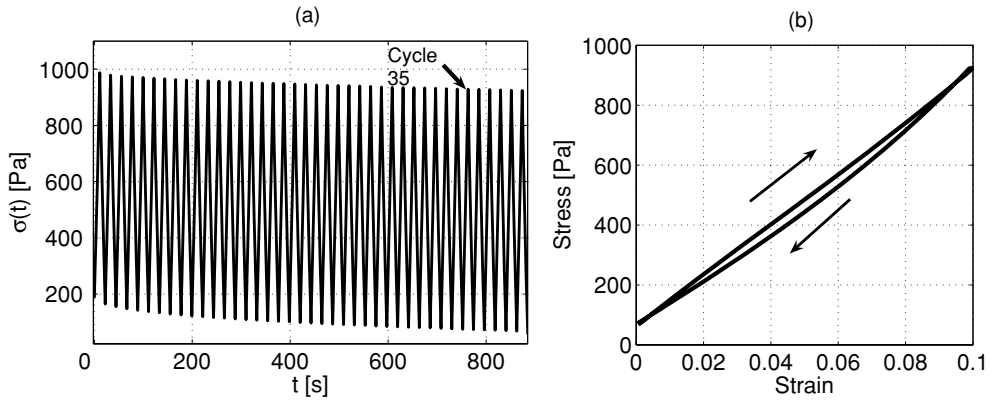

Figure 2. The stress versus time plot (a) of the stress–strain preconditioning on an IEP gel (pH 5.6) for 40 cycles. Part (b) displays cycle 40 of the stress–strain data used to estimate E_0.

and the sample during the unloading portion of the cycle. The pre-load also minimized displacement uncertainty due to loss in sample height. Analysis of the stress versus time data (figure 2) suggests that the transient effects of the gels are minimal after about 35 cycles, and the loading curve is approximately linear over the range of 10% engineering strain. Taking the slope of the loading portion of the 40th stress–strain curve provides an estimation of the elastic modulus (E_0) for each sample. Because of the transient response of the gel samples, this procedure was used to precondition all gel samples immediately before creep or stress relaxation measurements.

Creep curves were measured by applying a uniaxial stress of $\sigma_a = 720$ Pa to samples, while stress relaxation curves were recorded by applying a uniaxial strain of $\varepsilon_a = 0.08$. For both experiments, the stimulus was applied during a 1 s ramp and held constant for 3600 s. The output strain or stress data are processed under the assumption of a step input by shifting the first point of the output after the ramp to time = 0 s. The ramp data were disregarded. This approximation has a minor impact on the spectral response up to $\omega = 10^{-1}$ rad s^{-1} as described elsewhere (Sridhar and Insana 2007). Under this assumption the initial elastic response of each of these experiments provides an additional estimation of E_0.

3.5. Elasticity imaging measurements

Strain imaging experiments were performed on the pH injection phantoms described in section 3.3 in the form of an unconfined uniaxial creep test as described elsewhere (Sridhar *et al* 2007b). The bottom surface of the phantom was coated in oil to simulate free-slip boundary conditions, and the top surface was coated with an acoustic coupling gel. A flat plate that holds the ultrasonic transducer was attached to a motion controller. The motion controller was programmed to ramp up to the applied stress level (between 850 and 900 Pa) in 1 s and was held constant for 1800 s. A uniaxial stress was applied in the direction of the sound beam and normal to the top surface of the phantom. The stress was measured using a digital scale (Denver Instruments model TR-6101, Denver, CO) positioned beneath the phantom. The scale provided feedback to the motion controller for both applying and maintaining a constant stress. A photograph of the experimental setup is provided in figure 3.

RF echo data were acquired by a Siemens Sonoline-Antares system with the ultrasound research interface (URI) feature and a VF10-5 linear array transducer transmitting at 8 MHz.

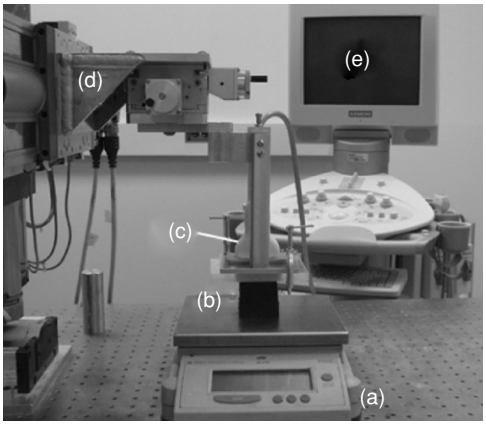

Figure 3. The experimental setup for elasticity imaging measurements described in section 3.5. The components are: (a) the digital scale, (b) the gelatin phantom, (c) the ultrasound transducer, (d) the motion controller and (e) the ultrasound system.

The RF frame rate was controlled through a waveform generator connected to the ECG trigger input. Data were acquired at four frames per second for the first 80 s and then at two frames per second for the final 1720 s. The initial acquisition rate is sufficient to capture the initial elastic response and short-duration viscoelastic responses. A pre-load strain of approximately 2–3% was applied to the phantom to ensure good acoustic contact with the transducer. Strain images were generated using the multi-resolution cross-correlation algorithm (Chaturvedi *et al* 1998).

3.6. pH indicator gels

An independent experiment using pH indicator solution (universal pH indicator system from Thermo Fisher Scientific, Waltham, MA) was performed as a way to independently assess the pH of the gel visually by colour contrast. This study was used to both validate that changes in viscoelastic properties were related to pH changes and to aid in the identification of the true pH distribution in the phantoms. Gelatin gels were manufactured according to the general procedure described in section 3.1. A set of gel samples was created by systematically changing the pH to 4.6, 5.6 and 6.6. Immediately following the addition of HCl or NaOH, 1% w/w pH indicator was added; the samples were thoroughly mixed and colour photographs were taken with a digital camera at $t_p = 48$ h. From the image data, a colour was assigned to each pH level.

A version of the elasticity imaging phantoms with HCl and NaOH injections was also created. The phantoms were prepared as described in section 3.3 except pH indicator solution (1% w/w) was added after the formaldehyde and graphite was omitted. After the HCl or NaOH was injected, the spatial variation in pH was tracked by observing colour variations. Photographs of these gels were taken at $t_p = 48$ h.

4. Results

4.1. Results of creep and stress relaxation measurements

Time- and frequency-domain methods were applied to creep and stress relaxation measurements of gel samples to estimate and interpret VE parameters with pH. In this section,

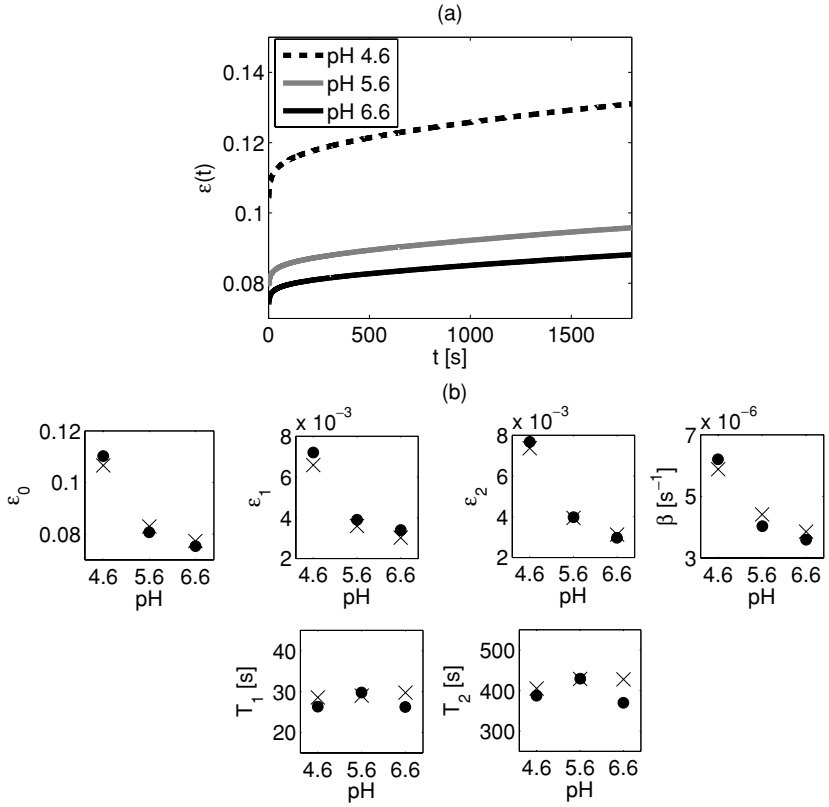

Figure 4. (a) Strain data for representative creep experiments on gel samples at pH 4.6, 5.6 and 6.6. (b) Row 1 provides the strain amplitude parameters and β for a tri-exponential Voigt model, and row 2 provides the VE time constants of the model. Results of two gel samples are displayed for each pH level with • corresponding to sample 1 and × corresponding to sample 2.

we describe the results obtained via these methods as well as a discussion of sources of systematic experimental error.

4.1.1. Time domain. Representative creep curves for gel samples at pH 4.6, 5.6 and 6.6 are displayed in figure 4. To find pH sensitive parameters, we fit the creep data to a tri-exponential Voigt model (figure 4). To be consistent with the acquisition time of the elasticity imaging measurements, we only used the first 1800 s of creep data for curve fitting. The Voigt model used in this study (section 2) contains the strain amplitude parameters ε_k that describe the elastic response, as well as time constants T_k that describe the viscous response to a constant mechanical stress. The $k = 3$ terms cannot be resolved with an acquisition time of 1800 s, thus they are represented by a single parameter β, which represents the first-order Taylor series expansion of the $k = 3$ VE Voigt element.

Based upon curve fitting results, it is clear that strain amplitudes decrease with pH, which corresponds to an increase in the elastic response with pH. However, this response is asymmetric about the IEP because a 1 pH unit decrease from the IEP causes a larger change in the strain amplitudes than a 1 pH unit increase. Also, the strain amplitudes (ε_0, ε_1, ε_2) and β are much more sensitive to pH than the VE time constants (T_1, T_2). Even though there are

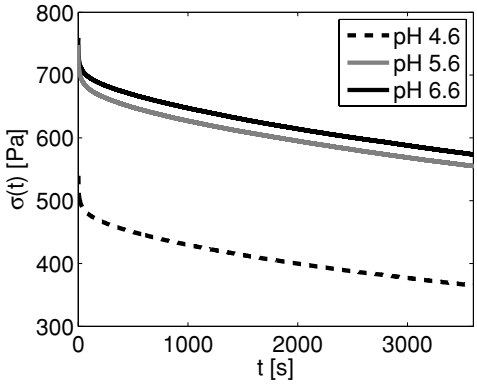

Figure 5. Stress data for representative stress relaxation experiments on gel samples at pH 4.6, 5.6 and 6.6.

Table 2. Average modulus $\bar{E}_0$ from stress–strain preconditioning measurements for the batches of gel stated. SD is the sample standard deviation.

Batch	$\bar{E}_0$ (kPa)	SD (kPa)	SD/$\bar{E}_0$%
pH 4.6	6.17	0.135	2
pH 5.6	8.33	0.167	2
pH 6.6	8.91	0.208	2

only two samples at each pH, similar results have been obtained in a previous investigation (Yapp *et al* 2007). Since pH variations in hydrogels were found primarily in the strain amplitudes and β, it is reasonable to focus the analysis of pH effects on ε_0 and β. Further analysis of the other exponential amplitude components is neglected because their amplitudes are approximately two orders of magnitude smaller than the ε_0 amplitude for gelatin gels, and therefore measurements of ε_1 and ε_2 have much higher percent errors than for ε_0. β is chosen for further analysis as well because it represents contrast evident at longer measurement times.

The time-domain results of representative stress relaxation data for different pH gels 4.6, 5.6 and 6.6 are displayed in figure 5. It is evident from the $\sigma(t)$ results that the initial elastic response ($\sigma(t = 0) = \sigma_0$) of the gel samples increases with pH in an asymmetric fashion about the IEP similar to that observed from the creep data.

As discussed in section 3.4, stress–strain preconditioning was performed on all gel samples prior to creep or stress relaxation measurements. This preconditioning provided a measurement of E_0 for each of the four gel samples at each pH level. These results are summarized in table 2 where $\bar{E}_0$ is the average modulus measurement of the four samples and SD is the sample standard deviation. E_0 was also estimated from the initial elastic response ε_0 and σ_0 of the creep and stress relaxation time-domain measurements, respectively. Thus we have three methods for estimating E_0 for each pH level. Because of systematic error due to thermal history (discussed in section 4.1.3) it is more useful to compare ratios of E_0 with respect to pH 5.6 in order to focus on contrast due to pH changes rather than sample variations. We define a parameter, $E_{\mathrm{CR}} = \frac{\bar{E}_0|_{\mathrm{pH}}}{\bar{E}_0|_{\mathrm{pH=5.6}}}$, to describe these ratios. The E_{CR} values corresponding to $\bar{E}_0$ measurements from stress–strain preconditioning, creep and stress relaxation measurements on gel samples are displayed in figure 6(a). A similar ratio approach is taken for analysis

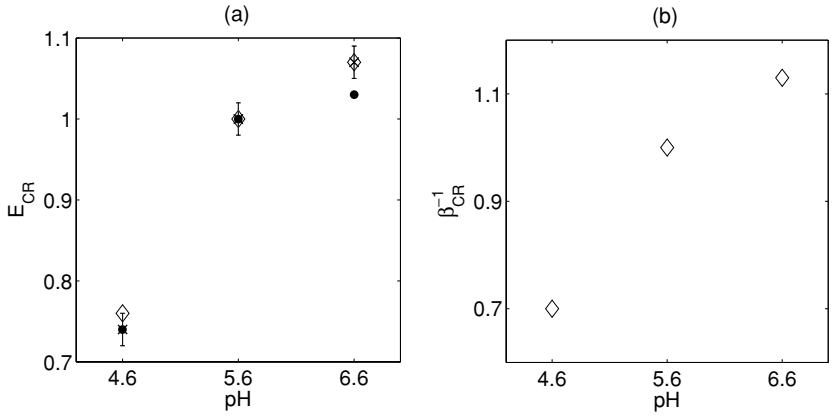

Figure 6. Part (a) displays E_{CR} values for $\bar{E}_0$ values for stress–strain preconditioning ($\times$), creep ($\diamond$) and stress relaxation ($\bullet$) measurements. The error bars on $\times$ data correspond to the SD/$\bar{E}_0$ values displayed in table 2. Part (b) displays β_{CR}^{-1} calculated from average β estimates from creep measurements.

of the β parameter determined from creep measurements. We define $\beta_{CR} = \frac{\beta|_{pH}}{\beta|_{pH=5.6}}$ for this purpose and plot results in figure 6(b). E_{CR} and β_{CR}^{-1} are ratios that describe quantities that are inversely proportional to a strain amplitude. The time-domain creep and stress relaxation measurements on gel samples provide two pH sensitive imaging parameters, E_{CR} and β_{CR}^{-1}. E_{CR} describes changes in the elastic modulus due to variation in instantaneous strain, while β_{CR}^{-1} describes long-term changes in the elastic response.

4.1.2. Frequency domain. Creep and stress relaxation measurements on gel samples provide independent estimates of $E^*(\omega)$ as described in section 2. For this frequency-domain analysis, the full 3600 s of data were used to maximize the frequency bandwidth. Representative storage $E'(\omega)$ and loss $E''(\omega)$ modulus spectra for pH levels 4.6, 5.6 and 6.6 for both creep and stress relaxation data are displayed in figure 7. Analysis of $E^*(\omega)$ spectra show that the storage modulus is much more sensitive to pH changes than the loss modulus, which is consistent with time-domain analysis.

4.1.3. Systematic error. We have observed that the thermal history of gelatin gels can be a major source of systematic error amongst gel sample sets. The thermal history of the gel includes all the temperature history from the time the gel was manufactured (the moment the gelatin and water were combined) until the time of testing. In these studies, the thermal history due to cooking the gel is well controlled; however, the storage temperature is dependent upon the room temperature of the laboratory. Thus, the storage temperature of the gels is the dominant source of systematic error due to thermal history in mechanical measurements. In this section, we describe ways to avoid bias when comparing across sample sets by studying the measurement variabilities. Three different batches, all at the IEP, are considered. The first two each contain four samples that polymerized under similar average storage temperature $\bar{T}$ conditions over t_p. $\bar{T}$ was determined by averaging the storage temperature recorded at three equally spaced time intervals over t_p. The third batch contained three samples that polymerized at a higher $\bar{T}$.

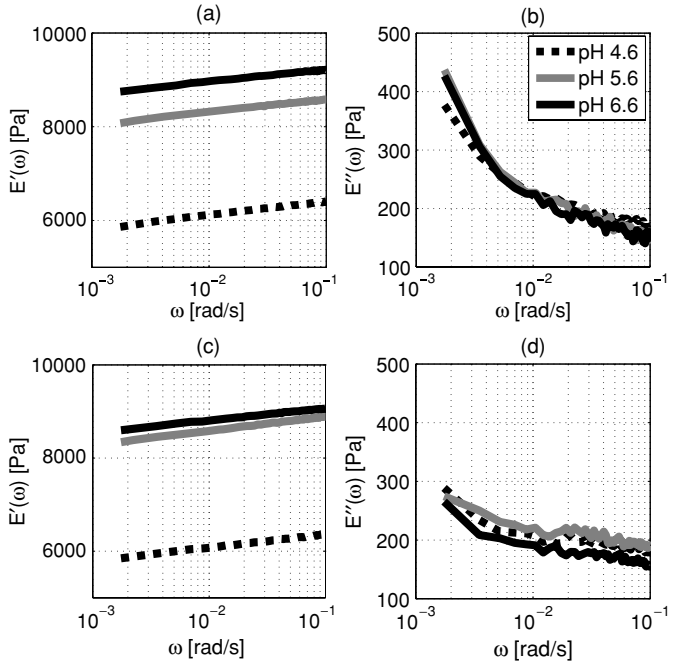

Figure 7. Parts (a) and (b) display the storage $E'(\omega)$ and loss $E''(\omega)$ modulus spectra, respectively, for the gelatin gels of pH 4.6, 5.6 and 6.6 as found from creep measurements. Parts (c) and (d) display the same spectra as found from stress relaxation measurements.

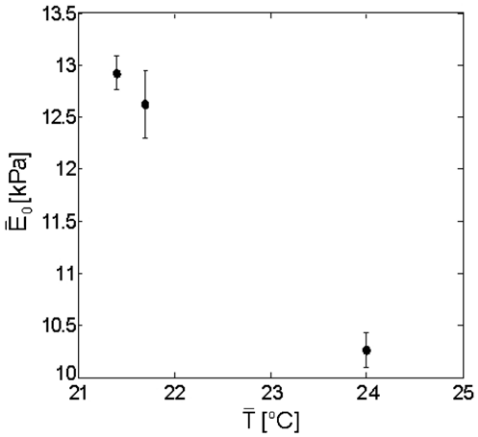

Figure 8. Variability in average elastic modulus $\bar{E}_0$ with average storage temperature $\bar{T}$. $\bar{E}_0$ values were determined from the 40th cycle of stress–strain preconditioning. The associated error bar is ± 1 sample standard deviation.

Figure 8 displays how the average elastic modulus $\bar{E}_0$ varies with $\bar{T}$ for the three batches. The results of this study indicated that E_0 measurements for gelatin gels are sensitive to modest variations in storage temperature. When all 11 samples from the three batches are considered as drawn from a single distribution, the sample standard deviation is 10% of $\bar{E}_0$. If only

the samples from the first two batches are considered, the sample standard deviation is 2%. These results indicate that it is important to maintain $< 1^{\circ}\mathrm{C}\,\bar{T}$ differences between gel sample batches to avoid systematic error in E_0 measurements.

4.2. Elasticity imaging

In this section, we describe the results obtained from elasticity imaging experiments described in section 3.5. As shown in figure 9(a), the standard ultrasonic B-mode image shows little to no contrast near the injection site. The procedure for imaging viscoelastic parameters is provided elsewhere (Sridhar *et al* 2007b). We obtained ε_0 images for all three phantoms, and a β image for the acid injection phantom as displayed in figures 9(b), (d) and (f) (ε_0 image for the control pH 5.6 phantom is not displayed). To evaluate elasticity pH imaging, an understanding of the mechanical properties of the gel under differing pH conditions is necessary, and the true pH of the inclusion must be known. To accomplish these tasks, the following two approaches have been taken:

(i) Use ε_0 and β images from gel phantoms to obtain E_{CR} and β_{CR}^{-1} parameters for comparison with creep and stress relaxation measurements.
(ii) Use the images of the pH indicator gels to predict the pH distribution in the gel phantoms.

To implement the first approach, a point-by-point inverse of the ε_0 and β images was taken to represent images approximately proportional to E_0 and β^{-1} images. The relationship is approximate because in practice the stress distribution is not spatially uniform. However, for the low strain contrast in this study, the inverse technique under the assumption of a uniform stress is a good approximation (Ponnekanti *et al* 1995). It is assumed that the pH of the background of the gel phantom is 5.6 when estimating E_{CR} and β_{CR}^{-1}. Lateral profiles of each image were taken from the average of the axial data in the outlined regions displayed in figure 9. Profiles are displayed in figures 9(c), (e) and (g).

The acidic phantom ε_0 image (figure 9(b)) shows local softening (bright strain), which corresponds to a reduced modulus as emphasized by the E_{CR} profile (figure 9(c)). This phantoms β image (figure 9(d)) also shows a brightening about the injection site. The corresponding β_{CR}^{-1} profile (figure 9(e)) gives a minimum of approximately 0.7. By comparing the E_{CR} and β_{CR}^{-1} profiles from the acidic phantom images to the E_{CR} and β_{CR}^{-1} values obtained from gel samples at pH 4.6 (figures 6(a) and (b)), we infer that the centre pH of the acid phantom is approximately 4.6. The pH increases outward from the centre of the injection until it reaches pH 5.6 resulting in a spatial distribution of pH covering approximately 1.5 cm.

The ε_0 image of the control pH 5.6 phantom (not displayed) and the corresponding E_{CR} profile (figure 9(c)) show some softening near the injection site, suggesting a structural weakening of the polymer as a result of excess fluid and tube withdrawal during polymerization.

The base injection phantom ε_0 image (figure 9(f)) and E_{CR} profile (figure 9(g)) indicate that the centre of the phantom is soft with an E_{CR} close to the background, but moving outwards from the centre a stiffening effect is observed. The E_{CR} values associated with the two peaks surrounding the centre in figure 9(g) are approximately twice the maximum E_{CR} measured with the creep and stress relaxation experiments in figure 6(a). The size of the base inclusion is larger than that of the acid inclusion with a diameter of approximately 2.5 cm. The differences in size of the inclusions and the high E_{CR} values observed in the base phantom may be the result of the gels enhanced buffering capacity to acids in comparison with bases. It was seen in table 1 that a much greater volume of acid was required to shift the pH of the gels to a lower value than the amount of base needed to shift the pH upward.

The second approach to the evaluation of pH-induced elasticity imaging is to estimate the pH distribution of the pH injection phantoms using colour contrast from gels with indicator

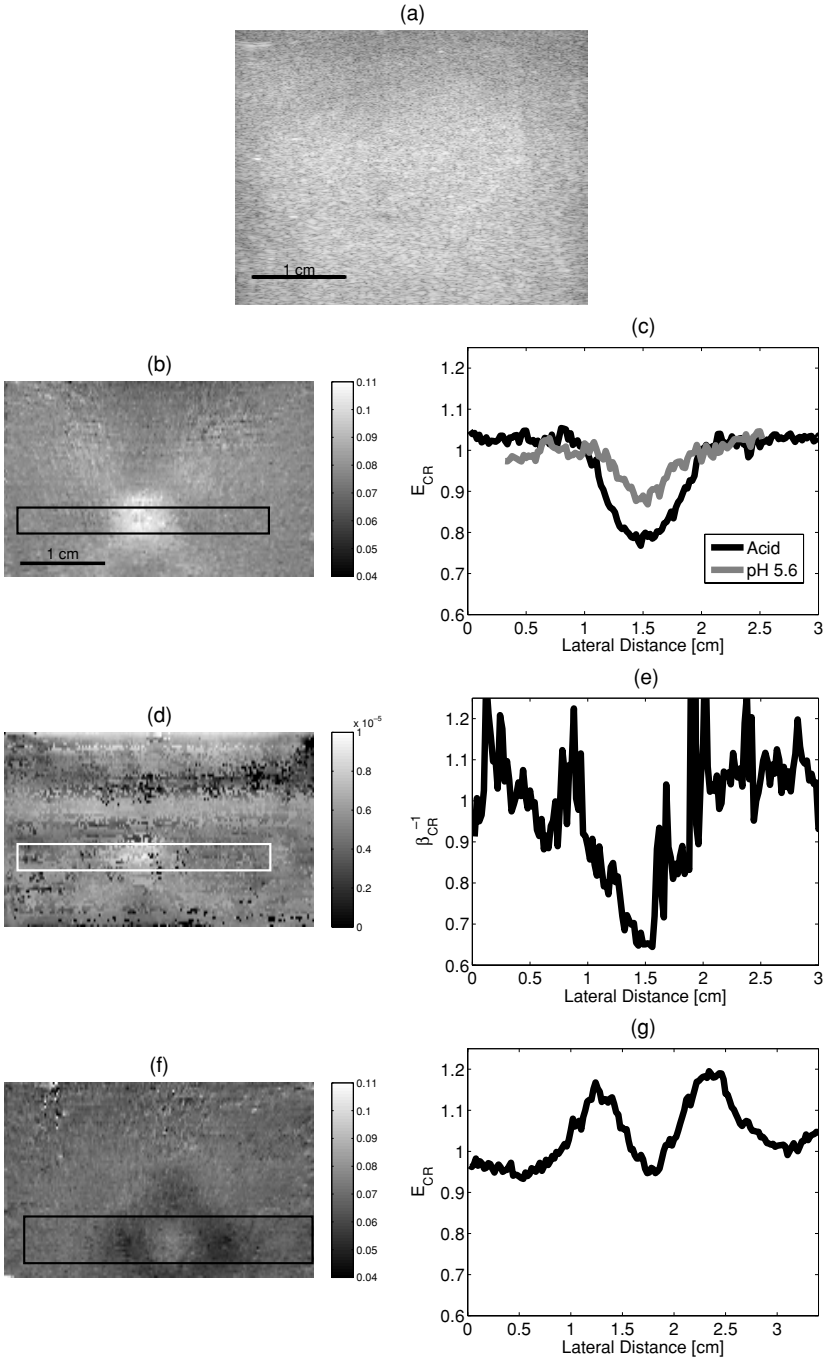

Figure 9. Part (a) is a representative ultrasonic B-mode image of an injection phantom. Part (b) is the ε_0 image of the acid injection phantom, and part (c) displays the corresponding E_{CR} profile relative to the background along with the E_{CR} profile for the control pH 5.6 injection (ε_0 image not shown). Part (d) is the β image of the acid injection phantom, and part (e) displays the corresponding β_{CR}^{-1} profile. Part (f) is the ε_0 image of the base injection phantom, and part (g) displays the corresponding E_{CR} profile. Rectangular regions in the images show the areas from which the profile plots to the right were obtained.

solution. To calibrate for the colours associated with different pH levels, individual gel samples were created with the pH indicator solution at the same three pH levels 4.6, 5.6 and 6.6 used for creep and stress relaxation measurements. Grey scale images provided the best contrast between pH 4.6 and pH 5.6 gels, and analysis of the red colours present in the RGB colour space provided the best contrast between pH 6.6 and pH 5.6. This analysis was first performed on the homogeneous pH indicator gel samples in order to find contrast standards for this study and then applied to the phantoms. Regions of each gel sample image were analysed by finding the mean and standard deviation of the colour intensity. Then contrast ratios of the mean values with respect to pH 5.6 were taken. To be consistent with E_{CR} and β_{CR}^{-1} measurements, the contrast ratios were normalized by the pH 5.6 gel values and therefore the more acidic gels measured less than one and the more basic gels measured greater than one. The contrast ratios are presented in figure 10(a).

Applying this same analysis technique to the injection gel phantoms with pH indicator solution (images displayed in figures 10(b) and (c)) requires the assumption that the background of the gel is pH 5.6. In a similar manner to the ε_0 image processing, lateral contrast ratio profiles from the selected region depicted on the images were analysed. The profiles, as seen in figures 10(d) and (e), in comparison with the contrast ratios presented in figure 10(a), suggest that the peak pH due to the acid injection is slightly lower than 4.6 and the width of this peak is approximately 2 cm. The basic injection gel phantom has a centrally located maximum pH with contrast approximately four times that found for the pH 6.6 colour contrast. The width of this peak is approximately 2.5 cm, which is in agreement with the width determined from the elasticity imaging study. The spatial distribution of pH in the heterogeneous gel phantoms is a result of a high concentration of acid or base diffusing outward from the centre of the injection site. Initially, the acid and base is very concentrated at the centre. At the time of injection the gelatin solution has not completely polymerized, thus the acid or base freely diffuses outward. The spatial change in pH between injection and measurement is not known; we only analysed the pH of the gel at $t_{\mathrm{p}} = 48$ h.

Because the basic injection gel phantom has contrast outside the range of the known pH contrast, it is likely that the pH at the centre of the phantom is much greater than 6.6. The pH indicator gel profile (figure 10(e)) does not have contrast minima located at the centre of the inclusion as it does for the E_{CR} profile in figure 9(g). This observation suggests that gels become softer when a critical pH level is exceeded; this type of behaviour was previously observed by Cumper and Alexander for type B gelatin gels with a similar IEP (Cumper and Alexander 1952). Rigidity (shear modulus) data reported by these authors have been reproduced in a modified version to represent E_{CR} contrast as seen in figure 11. In terms of E_0, it is reasonable to assume that contrast evident from the shear modulus (G) is the same as that for the initial elastic response of unconfined uniaxial compression under the assumption of an incompressible material such that $E_0 = 3G$ (Tschoegl 1989). Analysis of the data presented in Cumper's study suggests that G is maximum at approximately pH 10. The E_{CR} for pH 10 is about 1.2, which is the approximate maximum E_{CR} evident from the basic injection phantom (figure 9(g)). According to Cumper, the E_{CR} near pH 11 is similar to that of pH 5.6, thus it is reasonable to assume that the centre of the basic injection phantom has a pH near 11.

5. Discussion

Figures 4 and 7 show that the amplitudes of the VE Voigt units representing creep data are similarly affected by pH: in all cases strain decreases with pH as the gel stiffens. We also found that the VE time constants in figure 4 are insensitive to pH changes. Consequently, the

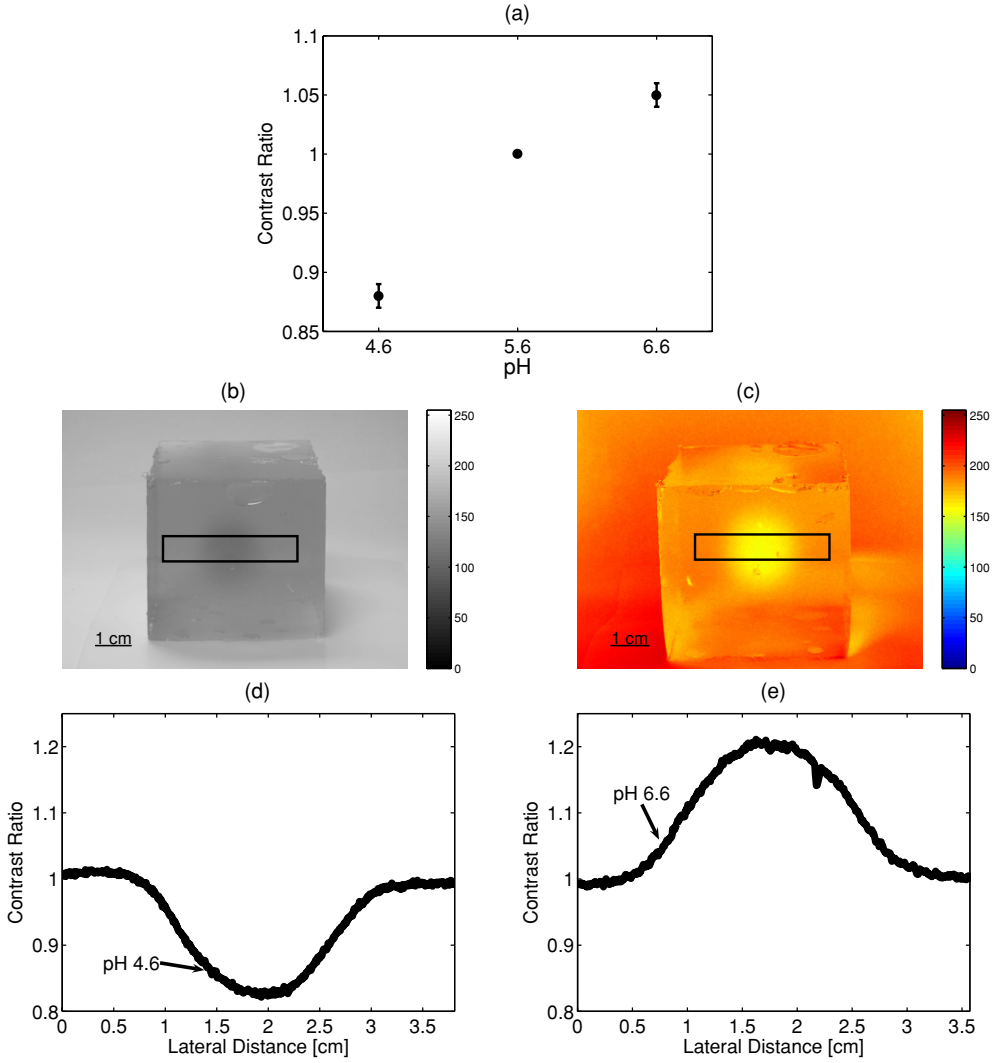

Figure 10. Part (a) displays the contrast ratios for individual pH values based upon the pH indicator solution contrast in gel samples. Part (b) displays the grey scale image of the acid injection phantom with pH indicator solution, and part (d) is the corresponding contrast ratio profile. Part (c) displays the red image of the base injection phantom with pH indicator solution, and part (e) is the corresponding contrast ratio profile.

(This figure is in colour only in the electronic version)

principle VE effects of pH on the hydrogel within ± 1 pH unit of the IEP appear to be elastic and not viscous.

Furthermore, in a study where finite-element model results were fit to gelatin hydrogel creep measurements for the unconfined geometry typical of elasticity imaging, we found that fluid motion in the gel occurs quickly (seconds) and is a relatively small component of the observed creep response (Kalyanam *et al*). This observation suggests that time-varying strain in hydrogels at any pH is dominated by elastic and viscoelastic responses of the collagen

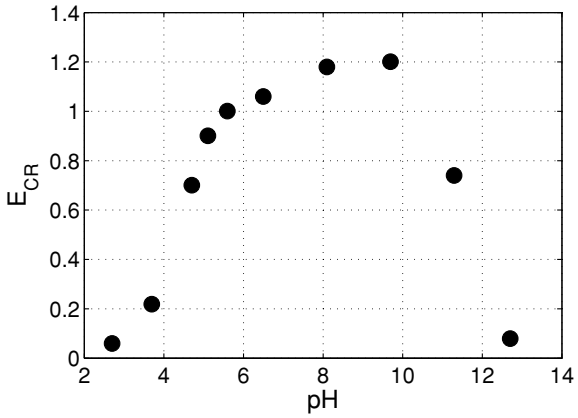

Figure 11. Approximate E_{CR} values versus pH from the original data of Cumper and Alexander (1952). The data presented in this figure are a modified version of that originally published by AJSR. The data value at pH 5.6 was not provided by Cumper and Alexander; we interpolated this value from the two data points surrounding pH 5.6. Permission to reproduce this modified version of the data was granted by CSIRO publishing. The full text of Cumper and Alexander's article can be accessed via either subscription or pay-per-view services at http://www.publish/csiro.au/nid/52/issue/3400.htm.

matrix more than the poroelastic response from fluid flowing through the matrix. Therefore, we should study how the collagen matrix changes with pH to understand the corresponding creep responses.

Individual fibres of type I collagen, as found in gelatin and breast stroma, deform elastically (Buehler and Wong 2007). However, the connections among fibres that determine hydrogel dynamics are primarily weak molecular bonds. These bonds regulate gel stiffness depending on the net electric charge density of the collagen molecules, and pH will affect the charge density.

The triple-helix structure of native collagen is stabilized internally by inter-chain hydrogen bonds and is efficient at cross linking with other helices (Gobeaux *et al* 2008, Bhattacharjee and Bansal 2005). Denatured forms of collagen, e.g. gelatin, have a lesser proportion of triple helices due to partial renaturation in the gel state (Djabourov 1988), and therefore gelatin gels are more fragile than native forms at the same collagen concentrations. Increasing pH above the IEP during gelation favours the formation of helical structures in gelatin gels (Mohanty *et al* 2007) that results in the greater storage modulus (Joly-Duhamel *et al* 2002) of the gel we observed at higher pH values. Decreasing the pH below the IEP has the opposite effect. In addition, IEP gels have the largest average molecular weight. Increasing or decreasing the pH from the IEP degrades the gelatin molecules, although the amount of degradation is greater for acidic gels (Mohanty *et al* 2007), resulting in shorter gelatin fragments. pH adjustments also induce structural changes in collagen (Usha and Ramasami 2000, Roeder *et al* 2002, Seehra and Silver 2006). Roeder *et al* (2002) found that an increase in pH produced fibrils of longer length, while a decrease in pH resulted in shorter collagen fibrils. The same study found that the elastic modulus increased with pH as a consequence of fibril length. Longer fibrils increase the mechanical integrity of the collagen network.

Similar modulus measurement trends were observed by Seehra and Silver (2006) when studying tissues subjected to pH changes. They attributed the enhanced modulus at basic pH to the high excess of net negative charges on a collagen molecule indicating that repulsive forces

between molecules may prevent flexible regions from deforming resulting in strain hardening. This combination of the change in average molecular weight, fraction of helical structures, charge density and polymer length with pH favours a predominantly elastic response to pH variations that we (figure 6) and others (figure 11) have observed in hydrogels.

Our hypothesis is that the pH effects on VE properties observed in hydrogels can serve as a model for pH effects on breast stroma elasticity. As a focal grouping of cancer cells rapidly grows beyond the capacity of the local blood supply, the extracellular pH in that region is reduced. Consequently, as tropocollagen segments emerge from stromal fibroblast cells, the acid conditions reduce their ability to self-assemble into long extracellular matrix fibres. We simulated the conditions of acidic breast stroma through changes in pH during gelatin polymerization. It is important to change the pH at the appropriate time in gel formation. We originally attempted to inject acids and bases into cross-linked gels, but quickly found that osmotic forces drew fluids to the injection site depending on the ionic concentration. Regardless of the pH we always found that the injection site was much stiffer than the surrounding gel. Changing pH during gelation gave an imaging response consistent with that of the uniform gel samples and the pH indicator gels.

In conclusion, at pH values in the range of ± 1 unit about the IEP, the elastic modulus of hydrogels increases with pH. For gelatin gels IEP = 5.6 and for collagen IEP $\simeq$ 7 (Usha and Ramasami 2000, Highberger 1939). The observed pH effects on mechanical properties are predominantly elastic, which is consistent with the literature describing how pH can influence the molecular structure of collagen. Although we did not specifically investigate the spatial resolution of elasticity imaging methods for detecting pH changes, the imaging results shown here suggest that the spatial resolution of pH-induced contrast is comparable to other important types of strain image contrast, such as variations in collagen density (Liu *et al* 2004). Insofar as gelatin hydrogel measurements mimic breast stroma, it seems that acidic breast tumours may be more detectable through contrast in elastic strain images than viscoelastic (time-varying strain) image properties, at least in the quasi-static bandwidth of force stimuli. We found recently that nonpalpable breast lesions can be classified as malignant or benign based on contrast in the time constant T_1, and that elastic strain was not discriminating between these classes (Qiu *et al* 2008). Under the assumption that our hydrogel model mimics the VE response of stroma, our observations suggest that extracelluar pH is not likely to be a diagnostic indicator for malignant–benign discrimination. Acidic tumours are more dangerous clinically and may have a lower elastic strain contrast than equivalent tumours of normal pH.

Acknowledgments

The authors would like to thank Peggy Qiu for her assistance with the curve fitting procedure for elasticity imaging, and David Mahr for his assistance with the instrumentation for elasticity imaging. Also, thanks to Rousselot Inc. for providing us with a generous supply of gelatin in support of this research. This work is based upon work supported by the National Cancer Institute under award number R0I CA082497.

References

Bhattacharjee A and Bansal M 2005 Collagen structure: the madras triple helix and the current scenario *IUBMB Life* **57** 161–72

Brown W H 2002 *Introduction to Organic Chemistry* 2nd edn (New Jersey: Wiley)

Buehler M J and Wong S Y 2007 Entropic elasticity controls nanomechanics of single tropocollagen molecules *Biophys. J.* **93** 37–43

Chaturvedi P, Insana M and Hall T 1998 Testing the limitations of 2-D companding for strain imaging using phantoms *IEEE Trans. Ultrason. Ferrorelectr. Freq. Control* **45** 1022–31

Cumper C W N and Alexander A E 1952 The viscosity and rigidity of gelatin in concentrated aqueous systems: II. Rigidity *Aust. J. Sci. Res. Ser. A: Phys. Sci.* **5** 153–9

Djabourov M 1988 Architecture of gelatin gels *Contemp. Phys.* **29** 273–97

Doyley M M, Sriivasan S, Dimidenko E, Soni N and Ophir J 2006 Enhancing the performance of model-based elastography by incorporating additional *a priori* information in the modulus image reconstruction process *Phys. Med. Biol.* **51** 95–112

Elenbaas B and Weinberg R A 2001 Heterotypic signaling between epithelial tumor cells and fibroblasts in carcinoma formation *Exp. Cell Res.* **264** 169–84

Fata J E, Werb Z and Bissell M J 2004 Regulation of mammary gland branching morphogenesis by the extracellular matrix and its remodeling enzymes *Breast Cancer Res.* **6** 1–11

Ferry J D 1980 *Viscoelastic Properties of Polymers* 3rd edn (New York: Wiley)

Fried J R 2003 *Polymer Science and Technology* 2nd edn (New Jersey: Pearson Education)

Garra B S, Cespedes E I, Ophir J, Spratt S R, Zuurbier R A, Magnant C M and Pennanen M F 1997 Elastography of breast lesions: initial clinical results *Radiology* **202** 79–86

Gerweck L E, Vijayappa S and Kozin S 2006 Tumor pH controls the *in vivo* efficacy of weak acid and base chemotherapeutics *Mol. Cancer Ther.* **5** 1275–9

Gillies R J, Raghunand N, Garcia-Martin M L and Gatenby R A 2004 pH Imaging *IEEE Eng. Med. Biol. Mag.* **23** 57–64

Gobeaux F, Mosser G, Anglo A, Panine P, Davidson P, Giraud-Guille M M and Belamie E 2008 Fibrillogenesis in dense collagen solutions: a physiochemical study *J. Mol. Biol.* **376** 1509–22

Hall T J, Bilgen M, Insana M F and Krouskop T A 1997 Phantom materials for elastography *IEEE Trans. Ultrason. Ferrorelectr. Freq. Control* **44** 1355–65

Highberger J H 1939 The isoelectric point of collagen *J. Am. Chem. Soc.* **61** 2302–3

Hitchcock D I 1931 The isoelectric point of a standard gelatin preparation *J. Gen. Physiol.* **14** 685–99

Joly-Duhamel C, Hellio D, Ajdari A and Djabourov M 2002 All gelatin networks: 2. The master curve for elasticity *Langmuir* **18** 7158–66

Kalyanam S, Yapp R D and Insana M F 2009 Poroviscoelastic behavior of gelatin hydrogels: implications for bioelasticity imaging *ASME J. Biomech. Eng.* at press

Khaled W, Reichling S, Bruhns O T and Ermert H 2006 Ultrasonic strain imaging and reconstructive elastography for biological tissue *Ultrasonics* **44** e199–202

Liu J, Abbey C K and Insana M F 2004 Linear approach to axial resolution in elasticity imaging *IEEE Trans. Ultrason. Ferrorelectr. Freq. Control* **51** 716–25

Mohanty B, Gupta A, Bohidar H B and Bandyopadhyay S 2007 Effect of gelatin molecular charge heterogeneity on formation of intermolecular complexes and coacervation transition *J. Polym. Sci.* B **45** 1511–20

Ophir J, Cespedes I, Ponnekanti H, Yazdi Y and Li X 1991 Elastography: a quantitative method for imaging the elasticity of biological tissues *Ultrason. Imaging* **13** 111–34

Pellot-Barakat C, Sridhar M, Lindfors K K and Insana M F 2006 Ultrasonic elasticity imaging as a tool for breast cancer diagnosis and research *Curr. Med. Imaging Rev.* **2** 157–64

Ponnekanti H, Ophir J, Huang Y and Cespedes I 1995 Fundamental mechanical limitations on the visualization of elasticity contrast in elastography *Ultrasound Med. Biol.* **21** 533–43

Qiu Y, Sridhar M, Tsou J K, Lindfors K K and Insana M F 2008 Ultrasonic viscoelasticity imaging of nonpalpable breast tumors: preliminary results *Acad. Radiol.* **15** 1526–33

Roeder B A, Kokini K, Sturgis J E, Robinson J P and Voytik-Harbin S L 2002 Tensile mechanical properties of three-dimensional type I collagen extracellular matrices with varied microstructure *ASME J. Biomech. Eng.* **124** 214–22

Seehra G P and Silver F H 2006 Viscoelastic properties of acid- and alkaline-treated human dermis: a correlation between total surface charge and elastic modulus *Skin Res. Technol.* **12** 190–8

Sharma A C, Soo M S, Trahey G E and Nightingale K R 2004 Acoustic radiation force impulse imaging of *in vivo* breast masses *IEEE Ultrason. Symp.* pp 728–31

Sinkus R, Siegmann K, Xydeas T, Tanter M, Claussen C and Fink M 2007 MR elastography of breast lesions: understanding the solid/liquid duality can improve the specificity of contrast-enhanced MR mammography *Magn. Reson. Med.* **58** 1135–44

Sinkus R, Tanter M, Xydeas T, Catheline S, Bercoff J and Fink M 2005 Viscoelastic shear properties of *in vivo* breast lesions measured by MR elastography *Magn. Reson. Imaging* **23** 159–65

Sridhar M and Insana M F 2007 Ultrasonic measurements of breast viscoelasticity *Med. Phys.* **34** 4757–67

Sridhar M, Liu J and Insana M F 2007a Elasticity imaging of polymeric media *ASME J. Biomech. Eng.* **129** 259–72

Sridhar M, Liu J and Insana M F 2007b Viscoelasticity imaging using ultrasound: parameters and error analysis *Phys. Med. Biol.* **52** 2425–43

Stoeckelhuber M, Stumpf P, Hoefter E A and Welsch U 2002 Proteoglycan-collagen associations in the non-lactating human breast connective tissue during the menstrual cycle *Histochem. Cell Biol.* **118** 221–30

Tanter M, Bercoff J, Athanasiou A, Deffieux T, Gennisson J, Montaldo G, Muller M, Tardivon A and Fink M 2008 Quantitative assessment of breast lesion viscoelasticity: initial clinical results using supersonic shear imaging *Ultrasound Med. Biol.* **34** 1373–86

Tschoegl N W 1989 *The Phenomenological Theory of Linear Viscoelastic Behavior* (New York: Springer)

Usha R and Ramasami T 2000 Effect of pH on dimensional stability of rat tail tendon collagen fiber *J. Appl. Polym. Sci.* **75** 1577–84

Veis A 1964 *The Macromolecular Chemistry of Gelatin* (New York: Academic)

Yapp R, Kalyanam S and Insana M 2007 Molecular and structural analysis of viscoelastic properties *Proc. SPIE Med. Imaging* **6511** 65111Y-1–65111Y-11